Session: 227
Economic Geology
#93240

$H_2O - CO_2 - CH_4$- BEARING FLUID INCLUSIONS IN QUARTZ: INSIGHTS INTO THE ORIGIN AND EVOLUTION OF TWO DIFFERENT HYDROTHERMAL AU DEPOSITS FROM THE EGYPTIAN EASTERN DESERT

ZOHEIR, B.A.[1], EL-SHAZLY, Aley K.[2], HELBA, H.[3], KHALIL, K.I.[3], and BODNAR, R.J.[4]
(1) Geology Department, Banha University, Banha, 13518, Egypt, (2) Geology Department, Marshall University, Huntington, WV 25725,
(3) Geology Department, University of Alexandria, Alexandria, Egypt, (4) Department of Geosciences, Virginia Tech, Blacksburg, VA 24061

Abstract
Shear-related, mesothermal gold deposits of Um Egat and Dungash in the Egyptian Eastern Desert are hosted by altered greenschist facies metavolcanic ± metasedimentary rocks of Pan-African age. Both deposits are similar in alteration style, structural control, and mineralogy. Gold is related to boudinaged quartz veins, where incipient recrystallization is common. Ore mineralogy includes pyrite, arsenopyrite ± pyrrhotite ± chalcopyrite ± galena. Au is disseminated in the alteration haloes, but also occurs in the veins as needles or blebs in fractures in altered arsenopyrite ± pyrite (Um Egat) or pyrrhotite (Dungash), usually next to fragments of altered country rocks.

Fluid inclusions in vein quartz occur in clusters, or along trails. Three types of fluid inclusions were identified based on preliminary microthermometry and laser micro-Raman spectroscopy: (i) three phase aqueous - carbonic (H_2O-CO_2±CH_4), (ii) two-phase carbonic (CO_2±CH_4±N_2), and (iii) two phase, CO_2-bearing, aqueous inclusions. Homogenization temperatures (T_h) for the two-phase carbonic inclusions fall in two distinct groups: > 300°C, and between 120 – 200°C, whereas for the two-phase aqueous inclusions, T_h is 120 to 200°C, and > 250°C. In all inclusions, the aqueous fluid has a low salinity (< 8 weight% NaCl equivalent). Inclusions from the same trail or cluster are often characterized by different degrees of fill or different T_h values.

Field, petrographic, and microthermometric data suggest that low salinity aqueous-carbonic fluids interacted with graphite – bearing metasediments to form CH_4. These reduced fluids leached Au as they circulated through the metavolcanics, carrying it as bisulfide complexes. A drop of pressure during the migration of these fluids to shallower depths led to phase separation. Interaction of these fluids with the country rocks precipitated Au - bearing sulfides. As in Arsenopyrite and Al in chlorite geothermometers constrain the conditions of Au precipitation between 340 and 250°C. Post depositional deformation caused the stretching, leakage, and decrepitation of some of the fluid inclusions increasing their T_h values to > 250°C, and remobilized the Au depositing it as globules of higher fineness in secondary sites.

Table 1: Geological setting of Auriferous Qz veins in Egat and Dungash

	Egat	Dungash
Host rocks	Metavolcanics + metasediments with arc signature; calcalkalic (old) and alkalic (young) granitoids.	Metavolcanics + metapyroclastics + metasediments of "older arc sequence (Shadli unit)"; calcalkalic (old) granitoids.
Metamorphism	Greenschist facies	Greenschist facies.
Host rock age	Between 711 and 600 Ma	711 ± 10 Ma
Vein type	Lenticular and boudinaged veins near contact with the young granites or dacite sills; fractured; milky Qz	One vein; boudinaged; and brecciated; milky Qz.
Vein size	Extends over 120 m; 0.6 – 4 m thick.	1.5 km long; 0.25 – 4 m thick.
Attitude	NNW – SSE shear zone	ENE – WSW shear zone (older structural trend).
Ore minerals:	Asp – Py ± Ccp ± Gn – Au	Py – Asp – Po – Pn – Spl – Gn ± Mar ± Mgt ± Au.
Au textures:	In altered Py and Asp; along fractures; as individual blebs in Qz	Inclusions in Py, Po, Asp, and Pn.
Grade (in veins)	0.3 – 40 ppm	3.87 ppm
Alteration	Distinct; < 0.8 m; sericite – chlorite – calcite – goethite ± dolomite ± pyrite	4 distinct zones; Au in carbonate + sericite zone.
Asp geothermometry	300 - 380°C	320 – 400°C
Chlorite geothermometry	220 - 270°C	300 - 325°C
T of veining	~ 340 – 250°C	~ 500 - 300°C

Introduction

Neoproterozoic rocks of the Arabian - Nubian shield exposed in the Eastern Desert of Egypt have long been known to host Gold, with more than 90 occurrences so far identified (e.g. Kochine and Bassuni, 1968; Botros, 2002; Fig. 1). Almost 25% of these occurrences are described as hydrothermal vein deposits crosscutting mafic and intermediate volcanics metamorphosed under greenschist facies conditions, and often intruded by intermediate to acidic rocks representing two discrete magmatic events (e.g. El-Ramly, 1970; Hussein, 1990; Hassan and Hashad, 1990; Botros, 2004).

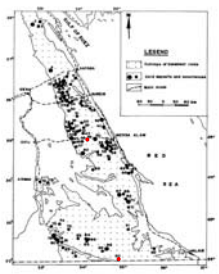

Fig. 1: Geological map of the Egyptian Eastern Desert showing the locations of 92 gold occurrences (after Kochine and Bassuini, 1968). The gold deposits of Dungash (46) and Egat (90) are highlighted in red.

Although most of these hydrothermal vein deposits were extensively mined between 1902 and 1958, their origin and conditions of formation remain controversial. Amin (1955) and Klumm et al. (2001) suggested that Au mineralization was related to the intrusion of the "younger (post-orogenic) granites" into older basement rocks between 620 and 530 Ma. Klumm et al. (2001) added that Au was deposited at T of 300 – 400°C and P of 1 - 2 kbar, a conclusion supported by Harraz (2000 & 2002) for the deposits at El-Sid and Atud (# 22 and 50, respectively, Fig. 1). Almond et al. (1984) suggested that Au deposition was related to an episode of shearing that post-dated the emplacement of all batholithic intrusions, but may have been coeval with regional cooling.

On the other hand, Hussein (1990) argued that most of these hydrothermal vein deposits are epithermal rather than mesothermal. In all cases, Au in these hydrothermal veins is considered to have been leached either from the intruded metabasalts, or from nearby ultramafic rocks. Although the source of the hydrothermal fluids leaching and transporting the Au may have varied from one area to another, most authors seem to favor either a metamorphic origin (e.g. Hassaan and El-Mezayen, 1995) or a combined metamorphic – magmatic origin (e.g. Harraz, 2000; Klumm et al., 2001; Botros, 2002; 2004). Addressing some of these problems requires detailed studies of the mineralogy and chemistry of the hydrothermal veins, careful analysis of the fluid inclusions in these veins, and stable isotope data.

Objectives of this study

1. To provide constraints on the minimum temperatures (and pressures) of veining for Au – bearing hydrothermal deposits from two different areas in the Eastern Desert of Egypt (namely, Dungash and Egat, Fig. 1).
2. To constrain the salinities of the vein forming fluids, and their compositions.
3. To provide models for the formation of the gold - bearing fluids at Dungash and Egat, particularly identifying whether they are orogenic or intrusion – related; mesothermal or epithermal.
4. To provide a better understanding of hydrothermal gold mineralization in general throughout the Egyptian Eastern Desert.

Geological Setting

In this study, hydrothermal vein deposits from two different areas (Egat and Dungash; Figs. 1 & 2) were selected for detailed petrological and microthermometric studies. Both deposits have many similarities in field relations, mineralogy, and texture, but have some differences, particularly in their structures. Table 1 lists the characteristics of these two deposits.

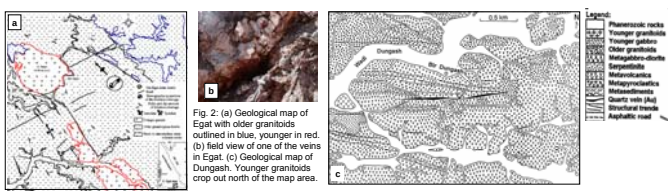

Fig. 2: (a) Geological map of Egat with older granitoids outlined in blue, younger in red. (b) field view of one of the veins in Egat. (c) Geological map of Dungash. Younger granitoids crop out north of the map area.

Petrography and mineral parageneses

Egat:
The quartz veins contain arsenopyrite (Asp) and pyrite (Py), with minor chalcopyrite and galena, all of which are almost always restricted to wall rock selvages along vein margins (Fig. 3a). Late goethite and siderite commonly replace Py and Asp in weathered portions of the vein and its wall rock. Gold most commonly occurs as irregular specks close to or included in Asp, along cracks in sulfides or their weathering products (Fig. 3b), or as blebs and globules (<20 µm) disseminated in the pervasively sericitized and chloritized wall rocks (Fig. 3c).

Fig. 3: Textural relations in Egat: (a) pseudomorphs of goethite after pyrite next of wall rock selvages. (b) Stringers of Au in goethite after Py/Asp; polarized reflected light; 320µm across. (c) Au specks in chlorite from the alteration zone.

Dungash:
The quartz vein contains pyrite, marcasite, pyrrhotite, chalcopyrite, galena and sphalerite. Except for sphalerite and marcasite, all these minerals also occur in the altered wall rocks, along with Asp, and minor pentlandite and gersdorffite ((Ni,Co,Fe)AsS). Gold occurs as: (i) inclusions in Asp (Fig. 4a) or disseminations in pentlandite, both within the sericite – carbonate zone of the wall rocks (Fig. 4b); (ii) as corroded inclusions in vein Py, and (iii) in microfractures of Py or along grain boundaries of Qz, especially next to the wall rock.

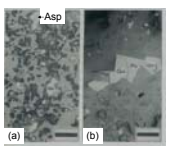

Fig. 4: Textural relations in Dungash: (a) Gold (Go) and arsenopyrite (Asp) disseminated in the carbonate – sericite zone of the altered wall rock. (b) Gold grain next to pentlandite (Pn) and galena (Gn) in altered wall rocks. Both photomicrographs taken under xpl; relected light. Scale bars: 0.5 mm.

Temperatures of vein formation and wall rock alteration

Textural observations and mineral chemical data indicate that these Au bearing vein systems have had a complex history involving wall rock alteration, fracture infilling, precipitation of vein minerals, and remobilization of Au. Estimating the T conditions of some of these stages is based on the application of geothermometers to minerals from the veins and alteration zones.

For Egat, electron microprobe analysis of arsenopyrite in the quartz veins yielded As contents of 28.4 to 30.9 wt.%. Application of the geothermometer of Kretschmar & Scott (1976) to this Asp - Py assemblage yields an average T of ~ 340 ± 30°C, with the fine grained, Au bearing variety yielding the lower T (~ 300°C) in that range (Fig. 5). On the other hand, chlorite from the extensively altered wall rocks is characterized by Al^{iv} of 1.9 – 2.3, and an Fe/Fe + Mg ratio of 0.35 – 0.52. Application of the geothermometer of Cathelineau (1988) to these analyses yields a T of ~ 220 - 270°C.

For Dungash, Khalil et al. (2003) concluded that veining and wall rock alteration took place over T of 500 - 300°C. The occurrence of Gersdorffite of composition $(Ni_{0.57}Co_{0.08}Fe_{0.35})AsS$ as an early phase within the altered wall rocks suggests that T of ~ 500°C prevailed during early alteration according to the experiments of Klemm (1965). Precipitation of Asp (29 – 31% As) + Po took place at T ~ 320 - 400°C based on the the geothermometer of Kretschmar & Scott (1976). On the other hand, the Al^{iv} content of chlorite geothermometer of Cathelineau (1988) yields a T of 308 - 325°C when applied to wall rock chlorite (Khalil et al., 2003).

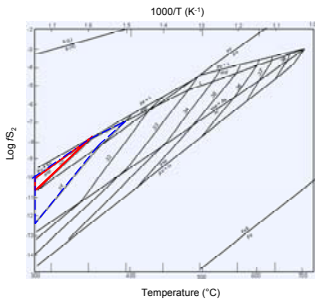

Fig. 5: Log fS_2 – T projection of the stability of Asp contoured for atomic wt% of As (Kretchmar & Scott, 1967). Red and blue lines delineate the conditions of formation of Asp in Egat and Dungash, respectively.

Fluid inclusion analysis

Analytical Techniques:
Fluid inclusion microthermometry was carried out on USGS gas flow type heating freezing stages at Rice University and the Fluids Research Lab, Virginia Tech. Analytical conditions are as in El-Shazly and Sisson (2004). Laser IR Micro-Raman Spectroscopic analysis was carried out at the Fluid Research Lab at Virginia Tech on a Jobyn Yvon Horiba LabRam-IR HR 800 Spectrometer. Counting time was 60 seconds for the first few analyses and 30 seconds for most routine analyses.

Petrography of Quartz veins:

Egat: Five samples of vein quartz were analyzed microthermometrically. R-10 is a quartz vein with selvages of altered wall rock and visible Au specks; R-20 and 24 are lenses of Qz from the alteration zones of a barren vein. R-21 and 22 represent younger barren quartz – carbonate veins. In all samples, Qz is elongated (~ 0.1 – 0.5 mm) with distinct subgrain boundaries oriented at a high angle to elongation (Fig. 6a). Incipient recrystallization along grain boundaries is common. Most fluid inclusions occur along trails that crosscut grain boundaries (Fig. 6b). Numerous decrepitated inclusions decorate the grain boundaries.

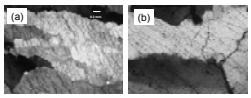

Fig. 6: (a) Elongated Qz grains with deformation bands and trails of secondary inclusions (R-22) (b) Fluid inclusion trails crossing grain boundaries; xpl; R-24. Field of view is 0.8 mm across.

Dungash: Three samples were selected for microthermometry. 324 and 326b are of milky vein quartz, with 326b more brecciated compared to 324. Sample 317 is a brecciated metavolcanic with a vein of quartz + calcite. Vein Qz is characterized by distinct fractures that run parallel to the elongation direction. Fluid inclusions occur along secondary trails crosscutting grain boundaries (Figs. 7a &b). Most inclusions are elongated in the direction of the trail (Fig. 7b).

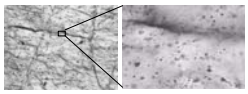

Fig. 7: (a) Fractured vein quartz from Dungash showing trails of secondary fluid Inclusions crosscutting grain boundaries. 324; ppl; 0.8 mm across. (b) Closeup of area outlined in (a).

Types of fluid inclusions:

Texturally, fluid inclusions occur (i) in clusters in the middle of the Qz crystals, (ii) along trails crosscutting grain boundaries, and (iii) along grain boundaries where they are decrepitated. Although many of the trails intersect, it is very difficult to determine their relative ages. Accordingly, we conclude that most trails formed more or less simultaneously either during or shortly after one of the deformational events affecting these veins. Most inclusions consist of two phases (liquid and vapor), but are often characterized by different degrees of fill (even within the same fluid inclusion assemblage, Fig. 8a). Based on preliminary microthermometry and laser micro-Raman spectroscopy, five types of inclusions were identified (Table 2):

Type	Size (μm)	Shape	Phases	Vol% vapor	Vapor comp.	T_h (°C)	Comments
A	< 12	equant	L + V	10 – 80	$CO_2 – CH_4 \pm N_2 \pm H_2O$	> 300	clusters or trails; Fig. 8a
B	< 12	equant	L + V	10 – 80	$CO_2 – CH_4 \pm N_2 \pm H_2O$	120 - 300	clusters or trails
C	< 10	spindle	L + V	10 – 20	$H_2O \pm CO_2$	120 - 200	trails; Figs. 8b
D	< 10	spindle	L + V	10 – 20	$H_2O \pm CO_2$	200 - 300	trails
E	12 - 20	irregular	2L + V	~20	$H_2O \pm CO_2 \pm CH_4$	NA	isolated or clusters, rare; Fig. 8c

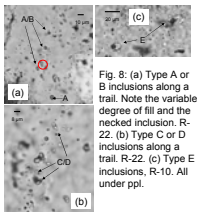

Fig. 8: (a) Type A or B inclusions along a trail. Note the variable degree of fill and the necked inclusion. R-22. (b) Type C or D inclusions along a trail. R-22. (c) Type E inclusions, R-10. All under ppl.

Microthermometry:

Egat: Most inclusions (> 60%) in R-10, R-20, R-21, and R-22 are carbonic (types A or B), with 10 - 35% types C or D, and < 5% type E. Temperatures of initial melting (Tm_e) for type A and B inclusions range from -68.5 to -54.2°C, with a median of ~ -64°C, those for types C and D range from -28 to -21°C. Final ice melting temperatures (Tm_f) range from -4.8 to 0°C, with most values > -3.5°C (Fig. 9). Clathrate melting temperatures (Tm_{clath}) were difficult to record and replicate, but generally range from 8.2 to ~ 17 °C (n= 31; median ~ 11 °C).

Homogenization temperatures (V → L) for type A inclusions vary considerably, with many inclusions failing to homogenize at T as high as 400°C. Most type B and D inclusions homogenize at 200 - 260°C, whereas typical values of T_h for type C were ~ 170°C (Fig. 10). In some samples (e.g. R-10, R-20), T_h values for inclusions in the same trail or fluid inclusion assemblage (FIA) differ by as much as 100°C. A few apparently aqueous inclusions in R-10 homogenize through the disappearance of the liquid (L → V).

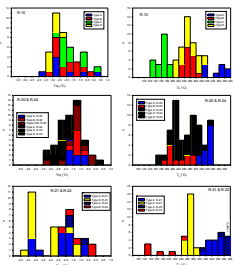

Fig. 9: Tm_f for Egat

Fig. 10: T_h for Egat

Dungash: More than 50% of all inclusions are aqueous-carbonic (types C or D), usually minute (~ 3 - 4μm), and elongated in the direction of their trail (Fig. 11a). 10 – 35% of all inclusions are negative crystals (types A or B), many of which are characterized by low degrees of fill (Fig. 11b). Thin walled, irregular aqueous inclusions constitute ~ 5 – 10% (Fig. 11c), whereas irregular, 3 – phase (type E; Fig. 11a) inclusions constitute another 5 - 10%. Tm_e range from -64 to -56°C for types A or B inclusions, and -44 to -21.2°C for types C and D. Tm_f values range from -3.8 to 0°C, although a few inclusions have values as low as -8.5°C (Fig. 12a). Final homogenization (V → L) for most type A & B inclusions occurs at T > 280°C. T_h values for most type C inclusions fall between 150 and 200°C, whereas those for type D inclusions are 220 - 280°C (Fig. 12b). T_h values for some inclusions from the same FIA differ by as much as 200°C. Several inclusions also homogenize through the disappearance of the liquid phase (L → V) at T ranging from 240 to 315 °C. One inclusion in 324 has a T_h of 17.8 °C.

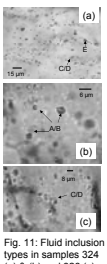

Fig. 11: Fluid inclusion types in samples 324 (a) & (b) and 326 (c); Dungash

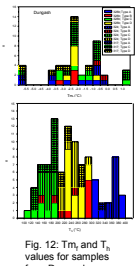

Fig. 12: Tm_f and T_h values for samples from Dungash.

Laser micro-Raman results:

Analysis of type A, B & E inclusions from samples R-10 and R-20 (Egat) revealed that the vapor phase contains CH_4+$CO_2 \pm N_2 \pm H_2O$ (Fig. 13a-c). N_2 is minor, and the CO_2/CH_4 is variable though always < 1. Type C & D inclusions are predominantly aqueous with minor CO_2. For the Dungash samples, type A, B inclusions contain CO_2, CH_4 and H_2O, whereas type C & D inclusions are aqueous with minor CO_2 (Fig. 14). Unlike the Egat samples, no N_2 was found in any of the carbonic inclusions, and the amount of CO_2 in these inclusions was far in excess of that of CH_4. No sulfur compounds or other hydrocarbons were detected in any of the samples analyzed.

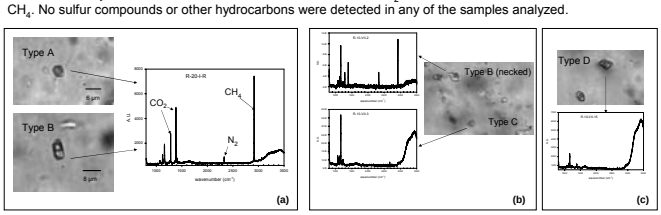

Fig. 13: Laser micro-Raman spectra for (a) type A and B inclusions; R-20; (b) types B and C inclusions; (c) Type D inclusions; R-10.

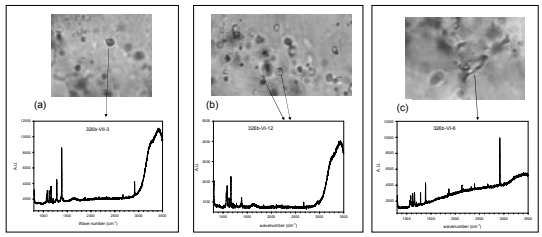

Fig. 14: Laser micro-Raman spectra for sample 326 (Dungash) (a) Type A; (b) Types C & D; (c) Type E.

Discussion and modeling of fluid compositions:

That both type B and D inclusions have similar T_h values (~ 250 ± 50°C) but different compositions suggests that they formed simultaneously in the same sample. Plots of T_h vs. Tm_f show that type B and D inclusions in both Egat and Dungash display weak negative trends, whereas data for type A inclusions are widely scattered (Fig. 15). This leads us to conclude that types B and D stretched and leaked, resulting in loss of H_2O (manifested by increased salinity) and an increase in volume (increased T_h), and that type A inclusions were derived from type B through these processes. Necking down (e.g. Figs. 8a & 13b), variable degrees of fill for the same FIA, and the fact that the smallest inclusions are characterized by some of the lowest Tm_f support this conclusion. On the other hand, the aqueous type C inclusions (T_h ~ 170°C) are interpreted to have formed at a later stage as suggested by their low salinity and occurrence along secondary trails only.

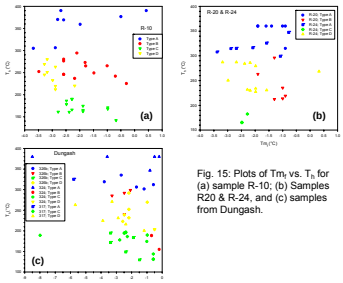

Fig. 15: Plots of Tm_f vs. T_h for (a) sample R-10; (b) Samples R20 & R-24, and (c) samples from Dungash.

Micro-Raman analysis of aqueous inclusions (C & D) combined with their Tm_e and Tm_f values suggest that these inclusions are filled with low salinity fluids belonging to the system NaCl – H_2O – CO_2. On the other hand, the fact that most of the carbonic inclusions (A & B) contain $CH_4 \pm N_2$, consist of a vapor and only one liquid phase (instead of 2), and have relatively high Tm_{clath} values (< 17°C, average~ 11°C), suggest that the amount of CH_4 was large enough (at least in Egat) to cause the disappearance of the three phase field (Diamond, 2003). That most of these carbonic inclusions have Tm_e values close to -64°C and an H2 type behavior (cf. van den Kerkhof and Thiery, 2001) also support this conclusion.

Fluid compositions for the aqueous inclusions were modeled based on their Tm_f, T_h and Vol% of the liquid using program "Bulk" of Bakker (2003) and the equations of state of Bowers and Helgeson (1983) and Bakker (1999). Both type C & D inclusions had very similar densities of 0.92 – 0.99 g/cm^3, and molar volumes of 19.6 – 21 cm^3/ mol. With the exception of the Dungash fluids being more saline, the compositions of these inclusions were almost the same from both areas with XCO_2 = 0.03 – 0.045, and XNa^+ < 0.027. Modeling the few odd inclusions which homogenized through the disappearance of the liquid (L→V) yielded compositions of XCO_2 = 0.12 – 0.26, XNa^+ < 0.003, and densities of 0.27 – 0.89. Isochores for these inclusions calculated using Bakker's (2003) program "Isochore" are shown in Fig. 16.

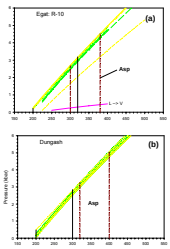

Fig. 16: Isochores for type C and D inclusions for: (a) Egat, and (b) Dungash. Green lines: Type C; Yellow lines: type D; pink isochore: inclusion homogenizing to vapor. Dashed red lines delineate the T of Asp formation, solid lines mark the T of entrapment of type D inclusions.

Attempts at modeling fluid compositions for type A and B carbonic inclusions using T_h and Tm_f values and program "Bulk" and assuming a vapor composition of: XCO_2 = 0.49, XCH_4 = 0.49, XN_2 = 0.02, for the Egat samples R-10 and R-20, and XCO_2 = 0.9, XCH_4 = 0.1 for Dungash samples failed to yield any meaningful results. However, both type B and D inclusions (T_h ~ 250°C) are assumed to have formed simultaneously following a stage of separation of the fluid into a CO_2 rich phase and an aqueous one. If we assume that the minimum T of entrapment of these fluids was ~ 250°C, the calculated isochores indicate a minimum P of entrapment of ~ 0.5 – 1.5 kbar for Egat and 1.2 – 1.6 kbar for Dungash (Fig. 16). For such P, available data on the CO_2 – H_2O - NaCl system (e.g. Crawford, 1981) and the effect of CH_4 on the miscibility gap (e.g. Diamond, 2003) indicate that XH_2O of the carbonic fluid would be < 0.3.

Origin and evolution of the Au deposits of Egat and Dungash

The Au deposits of Egat and Dungash can be classified as "orogenic" following Groves et al. (1998), as they both developed late in the orogenic cycle that formed the Arabian Nubian shield, and are not related to the granitic intrusions. Both deposits have so many similarities that their origins may broadly summarized in several stages:

1- Following regional metamorphism of arc related volcanics and their associated sediments under greenschist facies conditions, and the intrusion of the older granites, major shear zones developed, first in the ENE-WSW then in the NNW-SSE directions.
2- Circulation of hot, low salinity, aqueous fluids through the shear zones. These fluids were probably derived from the metavolcanics and metasediments, but may have been related in part to intruding magmas (younger granites). As these fluids migrated through graphite bearing schists, they formed CH_4 + CO_2 which remained completely miscible at the prevailing T. Small amounts of N_2 may have also been acquired from $(NH_4)^+$ bearing micas and feldspars in the country rocks. Migration of these fluids along the shear zones produced the observed alteration patterns.
3- As the aqueous-carbonic fluids migrated to shallower depths through the shear zones, they reacted with the country rocks precipitating Au-bearing sulfides (Py + Asp) at T ~ 400 – 320°C (Dungash) and 300 – 380°C (Egat). The drop of pressure associated with the opening/ widening of the shear zones and the upward migration of the fluids resulted in the separation of a carbonic-rich phase and an aqueous – rich one at T between 300 and 250°C, which may have in turn caused the precipitation of more sulfides. Quartz crystallizing within this T range trapped the carbonic and aqueous phases as discrete inclusions (types B and D) and at depths of ~ 6 - 9 km.
4- As the vein quartz straddled the brittle – ductile transition (~ 250°C; 2 – 3 kbar), it was deformed. Grain boundary migration, deformation banding and incipient annealing resulted in necking down, leakage, and decrepitation of some inclusions. This stage was probably accompanied by recrystallization of Asp and Py and the remobilization of Au and its precipitation along secondary sites.
5- As T and P dropped below 200°C, 2 kbar, microfractures developed in the vein Qz, and were subsequently healed trapping H_2O – rich fluids in type C inclusions. Later exhumation of the vein and country rocks caused stretching ± leakage of earlier formed inclusions as manifested by the higher T_h values recorded for type A inclusions and the overall scatter in T_h and Tm_f values.

Acknowledgements

This study was made possible by grants from the German Academic Exchange Service (DAAD) to BZ and KIK, and a research grant from ORGC at the University of Tennessee at Martin to AES. This work would not have been possible without the help and guidance of Dr. V. B. Sisson. The authors also acknowledge the technical support of Charles Farley with the micro-Raman analyses. Microprobe analyses were carried out on a CAMECA SX100 electron microprobe at the Institut fur Minerlaogie und Mineralisches Rohstoffe, Technische Universitat, Clausthal, Germany (Dungash samples), and a JEOL JSM-6310 electron microprobe at the Institute of Geology and Mineralogy, Graz University, Austria (Egat).